ELSEVIER

Journal of Power Sources 110 (2002) 73–79

JOURNAL OF POWER SOURCES

www.elsevier.com/locate/jpowsour

Effect of cobalt on the physicochemical properties of a simple LaB_5 metal hydride alloy

Renato C. Ambrosio, Edson A. Ticianelli*

Instituto de Química de São Carlos, USP, Av. do Trabalhador Sãocarlense, 400, Caixa Postal 780, CEP 13560-970, São Carlos, SP, Brazil

Received 30 March 2002; accepted 30 March 2002

Abstract

This work reports the results of a systematic study on the effect of Co as substituent for Ni on several physical and electrochemical properties of $LaNi_{4.7-x}Sn_{0.3}Co_x$ metal hydride alloys, where $0 \leq x \leq 0.7$. These included the unit cell lattice parameters measured using X-ray diffraction (XRD) and the electronic properties obtained using X-ray absorption spectroscopy (XAS). In general, the presence of cobalt in the alloys causes a decrease on the hydrogen equilibrium pressure and on the rate of capacity decay, and an increase in the cycle life and on the alloy activation time. A negligible effect of Co is observed in the maximum charge storage capacity and on the catalytic activity with respect to the hydrogen oxidation reaction (HOR). © 2002 Elsevier Science B.V. All rights reserved.

Keywords: Cycle life; Discharge capacity; X-ray absorption; Nickel-metal hydride battery

1. Introduction

$LaNi_5$-based hydrogen storage alloys with small substitutions of La and Ni have been extensively studied in the last years [1–9]. The main objective of the alloy modification is to increase the cycling life of metal hydride electrodes, but sometimes this causes an undesirable increase in the activation time and a decrease in the hydrogen storage capacity. Beneficial effects of substitution of La by Ce, Y, and Nd on the cycling life of metal hydride alloys have been reported [1,8,9]. In commercial AB_5-type metal hydride electrodes, quite good performance was obtained using mischmetal (Mm) in place of La, where Mm is a naturally occurring mixture of the rare earth metals, corresponding mainly to (in at.%): 50–55 Ce, 18–28 La, 12–18 Nd, and 4–6 Pr [1]. Since Ce is the predominant rare earth metal in normal Mm, the role of this element has been investigated in more detail [9]. Results indicated an improvement in the cycle life due to the presence of Ce, and this effect has been attributed to the formation of a passivating layer of oxide on the alloy particle surfaces.

Ratnakumar et al. [2] described the advantages associated with using Sn in $LaNi_5$ alloys, as a ternary substituent for Ni, in comparison to In, Ge, Si, and Al. Addition of small amounts of Sn improves the cycle life and the kinetics of hydrogen absorption and desorption, with a slight reduction in specific capacity. The optimal concentration of Sn in $LaNi_{5-x}Sn_x$ alloys was found to lie in the range $0.25 < x < 0.3$. Xue et al. [4] studied alloys with composition $MmNi_{3.6-}Co_{0.7-x}Al_{0.3}Mn_{0.4}Sn_x$. These studies have shown that inclusion of tin causes an increase in the hydrogen storage capacity and of the exchange current density for the hydrogen oxidation reaction (HOR), the optimal atomic fraction (x) of Sn being about 0.3.

The role of cobalt in the electrochemical properties of metal hydride alloys has been also the object of several works [4–7]. Studies have been conducted on several materials such as, $LaNi_4Co$, $LaNi_{3.5}CoAl_{0.5}$, and the more complex alloys, $LaNi_{3.55}Co_{0.75}Mn_{0.33}Al_{0.30}$, $LaNi_{4.3-x}Co_x$-$Mn_{0.4}Al_{0.3}$ ($x = 0$, 0.2, 0.4, 0.75) [4–7]. In all cases it has been observed that the main effect of Co is of improving the cycling life. This has been attributed to a diminution of the alloy corrosion caused by the formation of a Co-based surface passivation layer (i.e. surface oxide formation), and a smaller stress-cracking phenomenon due to a lowering of the alloy Vickers hardness [7] and/or to a smaller volume change upon hydrogen absorption and desorption [4–6].

This work reports the results of a systematic study on the effect of Co as substituent for Ni on several physicochemical properties of $LaNi_{4.7-x}Sn_{0.3}Co_x$ metal hydride alloys, where $0 \leq x \leq 0.7$. X-ray absorption spectroscopy (XAS) has been used to study the electronic properties of La, Co and Ni in the alloys, and X-ray diffraction (XRD) to characterize the

* Corresponding author. Tel.: +55-16-273-9945; fax: +55-16-273-9952.
E-mail address: edsont@iqsc.sc.usp.br (E.A. Ticianelli).

0378-7753/02/$ – see front matter
PII: S0378-7753(02)00239-2

crystal structure. Electrochemical studies included measurements of charge–discharge polarization characteristics, the cycling life, and charge–discharge reaction kinetics at several states of charge and temperatures. Kinetic studies of the hydriding–dehydriding processes have been made using electrochemical impedance spectroscopy. The hydrogen equilibrium pressure was monitored as a function of the state of charge on the activated electrodes.

2. Experimental

All alloys were prepared from commercial $LaNi_5$ alloy (Johnson Matthey) and cobalt and tin with purity superior to 99.9%, by the arc melting technique under inert gas. Ingots were re-melted four times and then annealed for 72 h in vacuum at 950 °C to ensure good homogeneity. Energy dispersive X-ray analyses (magnification 100×) made at several spots have confirmed within the experimental error the nominal composition of the alloys. XRD patterns were also obtained for each alloy. These experiments were performed in the 2θ range of 30–100° with steps of 3° min^{-1} using Cu Kα radiation. Alloy powders with a mean particle size <10 μm crushed by a mechanical method were used.

Electrodes were prepared by pressing a mixture comprised of 0.050 g of the alloy powder, 0.050 g of carbon black (Vulcan XC-72), and 33 weight percent (wt.%) polytetrafluoroethylene (PTFE) binder, on both sides of a nickel screen with a geometric area of 2 cm^2. Electrochemical measurements were done in a three-electrode cell in 6 mol l^{-1} KOH, with a Pt mesh counter electrode and an Hg/HgO-KOH 6 mol l^{-1} reference electrode.

Cycle-life tests were carried out by charging the electrode with a cathodic current of 10 mA (200 mA g^{-1} of the alloy) and discharging with an anodic current of the same magnitude to a cutoff cell potential of −700 mV versus Hg/HgO. Kinetic impedance measurements were made when the electrode charging capacity had reached the maximum. The electrochemical impedance spectra were recorded in the frequency range of 10 kHz to 1 mHz, with an ac amplitude of 5 mV, the electrodes maintained at open-circuit potential, on several states of charge and temperatures. For measurements of the hydrogen equilibrium pressure as a function of the state of charge, the activated electrode was fully charged and maintained at open-circuit until the potential reached equilibrium (variation of <0.1 mV min^{-1}). Then, the electrodes were partially discharged and the equilibrium potential measured again. This procedure was repeated until the electrode was fully discharged. The partial hydrogen pressures were calculated from the equilibrium potential (E^{eq}_{MH}) using the Nernst equation [10].

XAS measurements were conducted at the XAS beam line at the National Synchrotron Light Source (LNLS), Brazil. In this line, the radiation is monochromatized using Si(1 1 1) single crystal. The data acquisition set-up is comprised of three ionization chambers (incident I_0, transmittance I_t, and reference I_R detectors). The reference channel was primarily used for internal calibration of the edge position, using pure metal foils for Ni and Co and the uncycled $LaNi_5$ alloy powder for La. Analyses were carried out in the transmittance mode at the Ni K-edge and in the fluorescence mode at the Co K- and La L_{II}-edges due to the low concentration of these elements in the samples.

Samples for the XAS measurements were prepared by pressing a mixture of 20 mg of the alloy powder with 50 mg of Teflonized carbon, in a form of a disc with 1 cm^2 of geometric area. The computer program used in the analysis of the X-ray absorption data was the WinXAS package [11]. The X-ray absorption near edge structure (XANES) spectra were first corrected for the background absorption by fitting the pre-edge data (from −60 to −20 eV below the edge) to a linear formula, followed by extrapolation and subtraction from the data over the energy range of interest. Next, the spectra were calibrated for the edge position using the second derivative method, at the inflection point of the edge jump of the data from the reference channel. Finally, the spectra were normalized by taking as reference the inflection point of one of the extended X-ray absorption fine structure (EXAFS) oscillations.

3. Results and discussion

3.1. Structural and electronic properties

X-ray diffractometry was used to characterize the microstructure and measure the lattice parameters of the metal hydride alloys with different Co compositions. Fig. 1 shows the diffraction patterns for some $LaNi_{4.7-x}Sn_{0.3}Co_x$ alloys. XRD patterns confirmed that the alloys present a hexagonal $CaCu_5$-type structure. The diffraction peaks shift to smaller

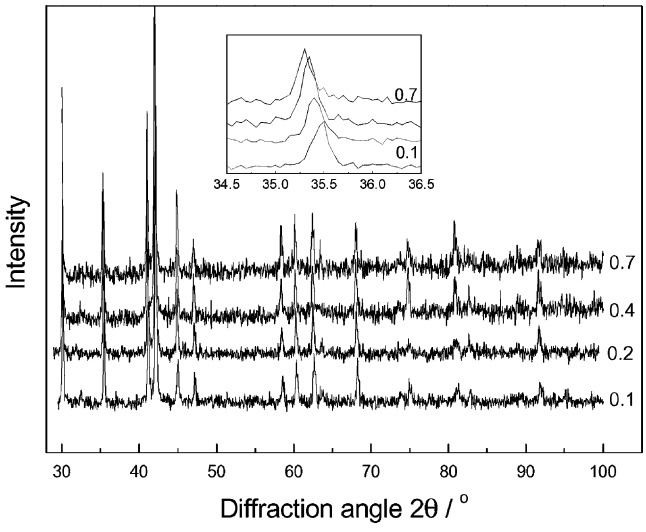

Fig. 1. X-ray diffraction patterns for $LaNi_{4.7-x}Sn_{0.3}Co_x$ alloys where 0.1, 0.2, 0.4, and 0.7 are the Co content (x) in the alloys. The inset shows the diffraction peak shifting to smaller angles with increasing Co content.

Table 1
Lattice parameters obtained by XRD, for the several alloys studied in this work, where a and c are the crystallographic axes in the hexagonal system and V is the unit cell volume

Material	a (Å)	c (Å)	V (Å^3)
$LaNi_{4.6}Sn_{0.3}$	5.058 ± 0.001	4.032 ± 0.002	89.4
$LaNi_{4.6}Sn_{0.3}Co_{0.1}$	5.062 ± 0.002	4.028 ± 0.002	89.4
$LaNi_{4.5}Sn_{0.3}Co_{0.2}$	5.070 ± 0.001	4.035 ± 0.002	89.8
$LaNi_{4.4}Sn_{0.3}Co_{0.3}$	5.064 ± 0.001	4.034 ± 0.001	89.6
$LaNi_{4.3}Sn_{0.3}Co_{0.4}$	5.078 ± 0.002	4.038 ± 0.002	90.2
$LaNi_{4.2}Sn_{0.3}Co_{0.5}$	5.078 ± 0.001	4.044 ± 0.002	90.3
$LaNi_{4.0}Sn_{0.3}Co_{0.7}$	5.080 ± 0.001	4.038 ± 0.001	90.3

angles due to the presence of cobalt in the alloy implying an increase of the lattice parameters. Table 1 summarizes the values of the unit cell volumes calculated using the XRD data. It is seen that the presence of cobalt in the alloy causes an increase in the a- and c-axes of the unit cell and, consequently, an increase of the cell volume. This increase is not proportional to the cobalt content and may indicate a partial segregation of cobalt in the alloys.

Figs. 2 and 3 show normalized XANES spectra at the Ni- and Co K-edges for several uncycled metal hydride alloys plotted together with those for the foil standards. Absorptions at the Ni- and Co K-edges are due to excitations of 1s electrons [12,13] to electronic states above the Fermi level. Because of the selection rule, only transitions into empty p states are allowed. Weak quadrupole allowed 1s–3d transitions may be observed as small pre-edge peaks in the XANES [13]. For Ni, theoretical calculations show that there is mixing of p and d states and as a result, transitions into the empty p-like part of these mixed p–d states can occur [12–14]. This is responsible for the appearance of the pre-edge peak at about 3.0 eV. In a series of metal hydride

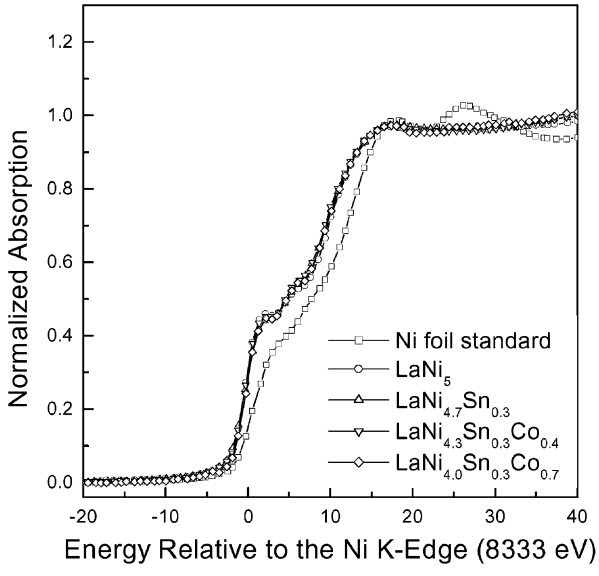

Fig. 2. XANES spectra in the transmission mode at Ni K-edge for uncycled alloys.

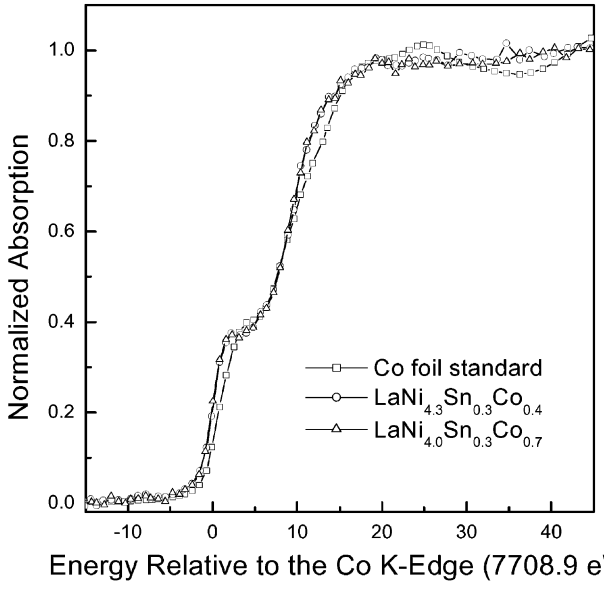

Fig. 3. XANES spectra in the fluorescence mode, at Co K-edge for uncycled alloys.

alloys in which the unit cell symmetry is maintained, the intensity of this pre-edge absorption feature can be taken as a measure of the occupancy of the p-like electronic energy states in the metal d-band [12–14].

XANES spectra for the Ni atoms (Fig. 2) in the alloys show that the magnitude of the pre-edge is not considerably affected by the presence of Sn and/or Co, as also observed for other AB_5-type alloys [1]. This means that substitutions of Ni for Sn and/or Co do not lead to any appreciable change in the energy of the Fermi level or in the occupancy of the p-like electronic states [12–14]. In Fig. 3, it is seen that at the Co K-edge, the position and magnitude of the pre-edge peak for the alloys are more similar to that for the Co foil standard. This indicates that the energy of the Fermi level and the occupancy of p-like orbital of Co do not suffer considerable change after alloying with La, Ni and Sn. This result may also be consistent with a partial segregation of the Co atoms, in which case the presence of a pure phase of Co with the same electronic properties and crystalline structure as in the pure foil may explain the spectral features.

XANES spectra at the La L_{II}-edge for the several uncycled metal hydride alloys are presented in Fig. 4. The most prominent spectral feature in the La L_{II}-edge is due to electronic transitions between the $2p_{1/2}$ and 5d energy levels [15]. The small increase in the intensity of this band observed for $LaNi_{4.7}Sn_{0.3}$ compared to $LaNi_5$ may be due to a decrease in the density of empty La 5d states, as observed for the case of $La(OH)_3$. This may arise as a consequence of a partial oxidation of the La in the sample or an electron captor effect of Sn. For the sample containing cobalt, the result is similar to $LaNi_5$ indicating that it is less oxidized than $LaNi_{4.7}Sn_{0.3}$. However, it should be emphasized that these differences are very small and may lie within the experimental error of the XAS analyses.

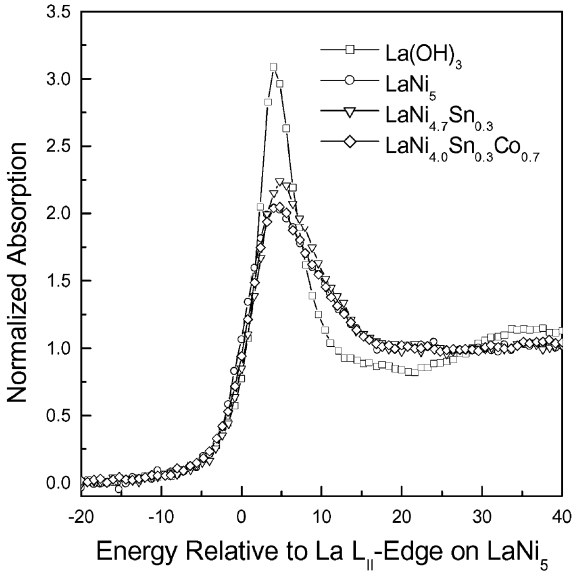

Fig. 4. XANES spectra in the fluorescence mode, at La L_{II}-edge for uncycled alloys.

In summary, from these measurements it is concluded that the most significant effect of Co in the structure of the metal hydride alloy is an increase of the unit cell volume. No significant electronic changes on the Ni or La atoms due to the presence of Co are detected.

3.2. Hydrogen adsorption isotherms

Fig. 5 shows the electrochemically-measured hydrogen equilibrium pressure plotted as a function of the state of charge of the electrodes. It is clear that for states of charge <80%, the hydrogen equilibrium pressure reaches a plateau and that the magnitude of plateau pressure is smaller for the samples containing larger amounts of Co. A diminution of the plateau pressure may be related with the formation of a stronger M–H bond and/or to a smaller compression of the H atoms inside the unit cell. Previous work has shown that the formation of hydride bond are preponderantly made through the Ni atoms [13,14]. XANES results indicated no significant change in the energy of the Fermi level or in the occupancy of the p-like electronic states of the Ni atoms due to the presence of Co. This implies that the Ni–H bond should have similar strength in all samples. Thus, the present results may only be explained by the rise of the unit volume introduced by cobalt, which would diminish the compression of H atoms, as also proposed by Adzic et al. [8] for other metal hydride alloys. In Table 1, a small difference in the lattice parameters is observed for the alloy with Co content of 0.1, compared to the alloys with Co contents of 0.4, 0.5, and 0.7 which have almost identical volumes. This fact seems to explain the similarities in the isotherm behaviors as seen in Fig. 5.

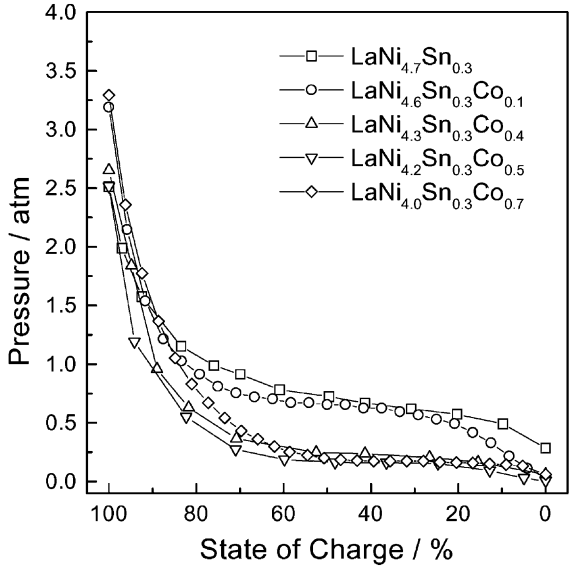

Fig. 5. Hydrogen equilibrium pressure vs. state of charge of the electrodes.

3.3. Alloy activation, charge storage capacity, and capacity decay

Fig. 6 shows the values of the discharge capacity, normalized to the maximum capacity, and plotted as a function of the cycle number for the several metal hydride electrodes. In Table 2, the values of the maximum capacity obtained in these experiments are reported. In Fig. 6, it is seen that in the first few cycles the electrodes are activated to reach the maximum charge storage capacity. An increase on the activation time due to the presence of cobalt is seen. It is also observed that the capacity decay after the maximum is linear with the cycle number, defining a rate of capacity

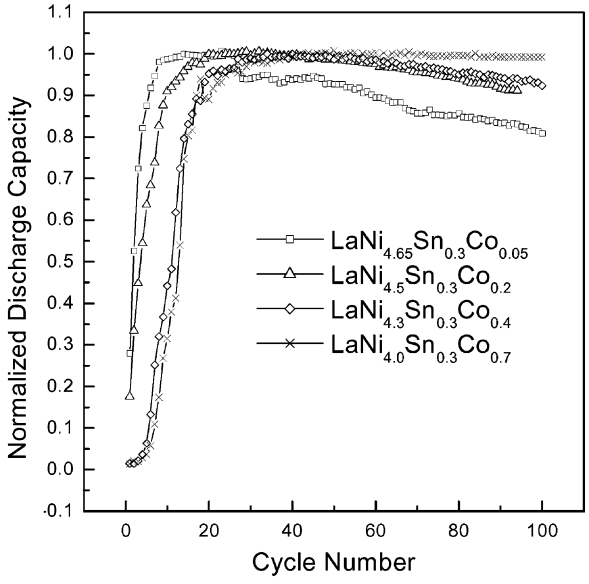

Fig. 6. Normalized discharge capacity vs. cycle number, obtained at a discharge current of 200 mA g^{-1} of alloy.

Table 2
Electrochemical parameters obtained for the different alloys electrodes

Material	Maximum capacity (mAh g^{-1})	$\left(\frac{dQ}{dn}\right)\frac{100}{Q}$ (%)	i_0 (mA g^{-1})
$LaNi_{4.65}Sn_{0.3}Co_{0.05}$	264	0.22	–
$LaNi_{4.6}Sn_{0.3}Co_{0.1}$	259	0.19	–
$LaNi_{4.5}Sn_{0.3}Co_{0.2}$	252	0.15	–
$LaNi_{4.4}Sn_{0.3}Co_{0.3}$	274	0.16	106
$LaNi_{4.3}Sn_{0.3}Co_{0.4}$	289	0.085	127
$LaNi_{4.2}Sn_{0.3}Co_{0.5}$	263	0.059	120
$LaNi_{4.0}Sn_{0.3}Co_{0.7}$	272	0.004	128

decay given by $dQ/dn = \text{constant}$, where Q is the normalized discharge capacity and n the cycle number. Table 2 presents these values for the different alloys, where it is seen that the rate of capacity decay clearly decreases as a function of Co content in the alloy, particularly for those with high Co content. For the alloy with a cobalt content corresponding to $x = 0.7$, the decrease of charge capacity is of the order of 0.4% after 100 charge–discharge cycles. Based on this, one would predict a capacity loss of only 4% after 1000 cycles, which is far below the degradation rate observed in practical metal hydride batteries.

In Table 2, no specific trend of variation of the maximum discharge capacity can be seen as function of Co content, the values being scattered ca. 4% around a mean value of 270 mAh g^{-1}. Taking into account the clear effect of Co on the other measured properties, this is a somewhat surprising result. However, it should be recognized that the maximum discharge capacity is an extensive property for the electrode, while all others are intensive. Thus, the dispersion of the maximum capacity can be associated to the dispersion of the alloy weight, and the effectiveness of anchoring onto the carbon substrate during electrode preparation. XANES results have shown that the electronic structure and the d band occupancy of Ni atoms in the alloys are essentially the same in the presence or absence of cobalt. As pointed out before [16], this would explain the similar charge storage capacity obtained as a function of Co content.

It is well accepted that the so-called activation process is a consequence of the reduction of the natural oxide covering the powder particles and of the decrease of the particle size caused by a stress cracking process due to the lattice expansion–contraction occurring upon hydride formation–decomposition [10]. On the other hand, the capacity decay observed after the maximum is usually attributed to the alloy pulverization and subsequent oxidation of the particle surface during the repeated charge–discharge cycles. XANES results for the uncycled samples do not indicate any appreciable change on the pre-edge intensity of Ni spectra or on the absorption hump of La caused by the presence of Co. Also, results show that XANES spectra of Ni, La, and Co atoms are those typically found for the elements in the reduced state (metallic form). These results show that the rise in the activation time introduced by Co cannot be related to a substantial rise on the initial surface oxide content of the alloy particles. Thus, the increase of the activation time seems to be more consistent with a slower rate of stress cracking.

As described in previous work [6], the activation time and the cycle life of the electrodes depend on the effect of hydrogen absorption on the structure of the alloy crystalline unit cell. It is known that the hydrogen absorption increases the lattice parameters and induces a phase transition from a α-phase to a β-phase in which the pressure–concentration curve (Fig. 5) exhibits a plateau [7]. This induces a large mechanical tension on the phase boundaries, where unit cells with different sizes are joined together, making the alloy disintegrate into a powder even during the first hydriding cycle. According to Adzic et al. [6], the presence of Co in AB_5 alloys significantly improves the cycle life by reducing the partial molar volume of hydrogen in the alloy lattice, reducing the cell expansion and the stress cracking. Another consequence of the Co is an increase on the oxide coverage on the cycled alloy causing a surface passivation and an increase of stability by decreasing the exposure of the active material to the alkaline corrosive electrolyte [6]. Finally, Chartouni et al. [7] observed that the substitution of Ni by Co lowers the Vickers hardness of the alloys, which also may account for the increase of stability over repeated charge–discharge cycles. All these phenomena can contribute to enhancing the stability of the alloys with high Co concentrations, as observed in the present investigation.

3.4. Kinetics of the hydriding–dehydriding processes

Fig. 7 shows the electrochemical impedance spectra for the activated $LaNi_{4.0}Sn_{0.3}Co_{0.7}$ alloy, obtained at several temperatures for a fully charged electrode. Fig. 8 shows

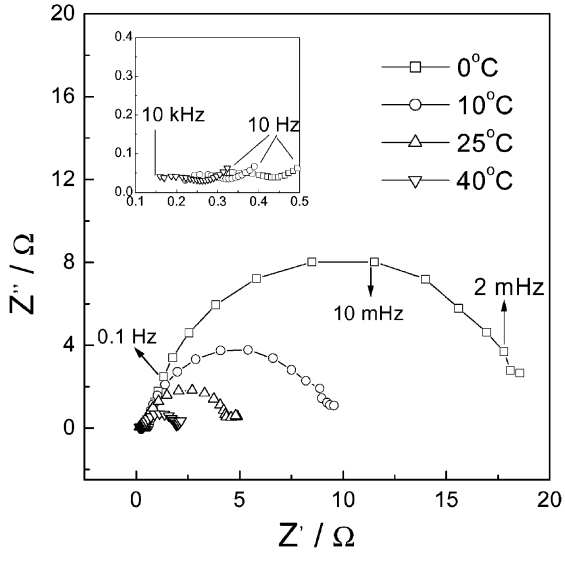

Fig. 7. Nyquist plots at several temperatures of $LaNi_{4.0}Sn_{0.3}Co_{0.7}$ fully charged electrode. The inset shows the arcs in the high frequency range.

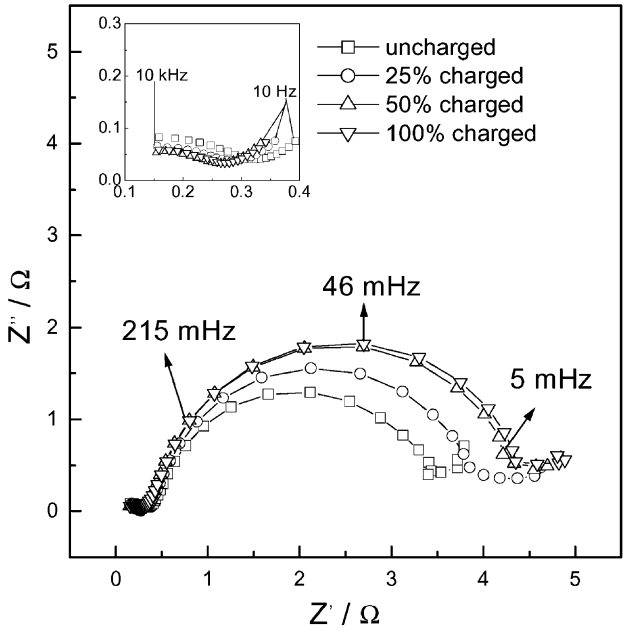

Fig. 8. Nyquist plots at several states of charge of $LaNi_{4.0}Sn_{0.3}Co_{0.7}$ electrode at 298 K. The inset shows the arcs in the high frequency range.

the impedance plots for the same alloy at several states of charge. It should be noted that these impedance responses are qualitatively similar to results presented for other metal hydride alloys [1,17]. It is observed that in high-frequency range the impedance spectra show an arc with the magnitude and characteristic frequency essentially independent of the temperature and state of charge (insets in Figs. 7 and 8). In the lower frequency region, another arc is developed but here the features are strongly dependent on the temperature and the state of charge of the electrode.

The arc in the high frequency range can be associated to a contact resistance between the current collector and the active material [1]. The small increase in the magnitude of the arc with the decrease of the state of charge (inset in Fig. 8) can be explained by an increase in the contact resistance resulting from the volume contraction of the metal hydride particles occurring upon alloy discharge. The low frequency arc can be assigned to a relaxation associated with the rate-determining step of the hydriding–dehydriding process, which in principle can be either the diffusion of absorbed hydrogen,

$$\text{S-H}_{\text{abs(bulk)}} \rightleftharpoons \text{S-H}_{\text{abs(surface)}} \quad \text{(diffusion)} \tag{1}$$

or, the charge transfer step,

$$\text{S-H}_{\text{ads}} + \text{OH}^- \rightleftharpoons \text{H}_2\text{O} + \text{S} + e^- \quad \text{(charge transfer)} \tag{2}$$

From the fact that the magnitude of the arc is smaller for the discharged electrode, for which (if present) the diffusion problem should be enhanced, it is concluded that this feature must be assigned to the charge transfer step. Thus, the exchange current density (i_0) for this step can be evaluated from the radius (R_{ct}) of this arc, using the Butler–Volmer equation in the limit of low overpotentials, that is,

$$i_0 = \frac{RT}{nF}\left(\frac{1}{R_{ct}}\right) \tag{3}$$

where F is Faraday's constant, R the gas constant, and T the temperature. Values of i_0 obtained for some of the metal hydride electrodes at 25 °C, 100% state of charge, are presented in Table 2. Also, i_0 measurements were conducted at several temperatures in order to obtain the activation energy of the hydrogen oxidation step (reaction (2)). The values of the activation energy for several cobalt contents resulted scattered ca. 2% around a mean value of 36.3 kJ mol^{-1}. Thus, within experimental error, the activation energy is independent of the Co content. Based on this fact, it is concluded that the small differences in the exchange current density, as observed in Table 2, may be merely a consequence of the different average surface area of the alloy particles.

Reaction (2) shows that a crucial step for the hydrogen oxidation electrocatalysis is the breaking of the S–H bond, which should be formed from hybridization of d electrons of Ni and the 1s electron of the hydrogen atom [13,14]. A more filled d band will imply that the hybridization with the 1s electron of the hydrogen atoms will involve fewer bonding electrons, leading to the formation of weaker Ni–H bonds [18]. In the present cases, XANES results in Fig. 2 do not indicate any difference in the electronic structure of the Ni atoms in the alloys containing different amounts of cobalt. This fact can explain the similarity of the values of the exchange current density and activation energy for the alloys studied in this work.

4. Conclusions

Electrochemical experiments were conducted on metal hydride electrodes to analyze the effects of the Co content on the properties of a AB_5-type metal alloy electrodes. In general, the presence of cobalt on the alloys in high concentration causes a decrease on the hydrogen equilibrium pressure and on the rate of capacity decay, and an increase in the cycle life and on the alloy activation time. A negligible effect of Co content is observed over the maximum charge storage capacity.

An expansion of the unit cell volume occurs due to the presence of Co, particularly for high Co content. Since the maximum charge storage capacity is not changed, this led to a smaller compression of the hydrogen atoms (or a lower molar volume) and as a consequence a diminution of the hydrogen equilibrium pressure. This may also have led to a decrease in the stress cracking process, thus, raising the stability of the materials.

The low frequency impedance features of the metal hydride electrodes were related to the charge transfer step

of the hydriding–dehydriding processes. It was found that the catalytic activity with respect to the HOR is essentially independent on the Co content.

XANES experiments indicated a negligible effect of Co on the electronic properties of the La and Ni atoms, implying in the formation of similar strength metal–hydrogen bond. This explains the similar charge storage capacity and the hydrogen reaction kinetics for the alloys with different amounts of cobalt.

Acknowledgements

The authors wish to thank FAPESP, CAPES, FINEP, CNPq, and the National Synchrotron Light Source (LNLS), Brazil for financial supports.

References

[1] E.A. Ticianelli, S. Mukerjee, J. McBreen, G.D. Adzic, J.R. Johnson, J.J. Reilly, J. Electrochem. Soc. 146 (1999) 3582.
[2] B.V. Ratnakumar, C. Witham, R.C. Bowman Jr., A. Hightower, B. Fultz, J. Electrochem. Soc. 143 (1996) 2578.
[3] C. Witham, B.V. Ratnakumar, R.C. Bowman Jr., A. Hightower, B. Fultz, J. Electrochem. Soc. 143 (1996) L205.
[4] Q. Xue, G. Xueping, C. Jiansheng, Y. Huatang, S. Deying, in: Proceedings of the 13th World Conference on Hydrogen Energy, Beijing, China, 12–15 June 2000, p. 960.
[5] G.D. Adzic, J.R. Johnson, S. Mukerjee, J. McBreen, J.J. Reilly, J. Alloys Comp. 253/254 (1997) 579.
[6] T. Vogt, J.J. Reilly, J.R. Johnson, G.D. Adzic, J. McBreen, J. Electrochem. Soc. 146 (1999) 15.
[7] D. Chartouni, F. Meli, A. Züttel, K. Gross, L. Schlapbach, J. Alloys Comp. 241 (1996) 160.
[8] G.D. Adzic, J.R. Johnson, J.J. Reilly, J. McBreen, S. Mukerjee, M.P.S. Kumar, W. Zhang, S. Srinivasan, J. Electrochem. Soc. 142 (1995) 3429.
[9] M.P.S. Kumar, W. Zhang, K. Petrov, A.A. Rostami, S. Srinivasan, G.D. Adzic, J.R. Johnson, J.J. Reilly, H.S. Lim, Electrochem. Soc. 142 (1995) 3424.
[10] P.H.L. Notten, M. Latroche, A.P. Guégan, J. Electrochem. Soc. 146 (1999) 3181.
[11] T. Ressler, J. Phys. IV C2 (1997) 269.
[12] B. Lengeler, R. Zeller, J. Less-Common Met. 103 (1984) 337.
[13] M. Gupta, J. Less-Common Met. 130 (1987) 219.
[14] D.A. Tryk, I.T. Bae, Y. Hu, S. Kim, M.R. Antonio, D.A. Scherson, J. Electrochem. Soc. 142 (1995) 824.
[15] D.A. Scherson, Electrochem. Soc. Interf. 5 (1996) 34.
[16] S. Mukerjee, J. McBreen, J.J. Reilly, J.R. Johnson, G. Adzic, K. Petrov, M.P.S. Kumar, W. Zhang, S. Srinivasan, J. Electrochem. Soc. 142 (1995) 2278.
[17] W. Zhang, M.P.S. Kumar, S. Srinivasan, H.J. Ploehn, J. Electrochem. Soc. 142 (1995) 2935.
[18] J.M. Jaksic, N.M. Ristic, N.V. Krstajic, M.M. Jaksic, Int. J. Hydrogen Energy 23 (1998) 1121.